

Seismic Behavior of Shear-Critical Reinforced Concrete Frame: Experimental Investigation

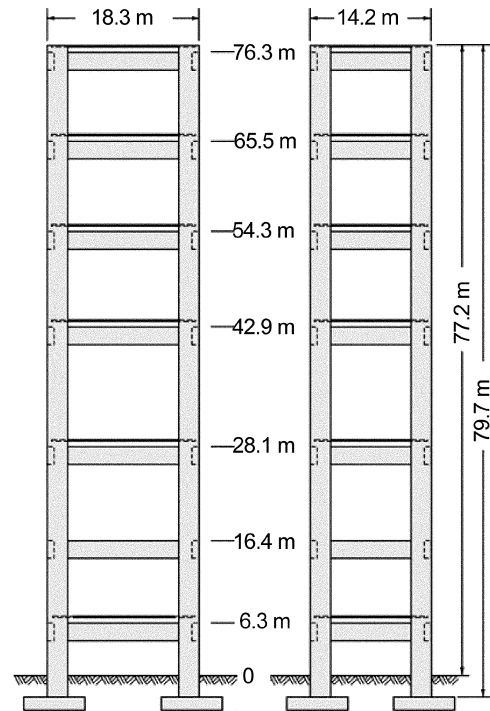
by Kien Vinh Duong, Shamim A. Sheikh, and Frank J. Vecchio

Many reinforced concrete structures that were built approximately 40 years ago or earlier, and some built much more recently, were done so without adequate consideration for shear-critical behavior under seismic conditions. Such buildings are of great concern because, in the event of an earthquake, they may fail in a brittle and catastrophic manner. Unlike with moment-critical structures, the behavior of structures that are shear-critical under seismic load conditions has not been well studied. An experimental investigation was carried out to examine the behavior of a shear-critical reinforced concrete frame under seismic loading. A single-span, two-story, reinforced concrete frame with shear-critical beams was constructed and tested in a lateral reverse cyclic manner until severe shear damage took place in the beams. The beams were then repaired with carbon fiber reinforced polymer (CFRP), and the frame was retested. The damage mode in the beams after repair changed from shear- to flexure-controlled. In addition, substantial improvements were observed in overall peak lateral load, ductility, maximum displacement, and energy dissipation. The experimental findings concluded that CFRP wrap can be a simple and effective means of repair of shear-deficient frames, and that the CFRP strain limitations proposed by ISIS Canada are conservative.

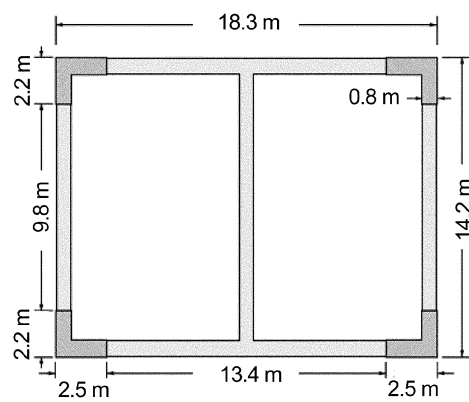
Keywords: ductility; frames; rehabilitation; reinforced concrete; shear.

INTRODUCTION

Over the past several decades, structural engineers have made great advances in understanding the seismic behavior of structures. This knowledge, combined with improved modern-day practice, enables us to not only design buildings that can safely withstand severe earthquake loads without collapse, but also to design buildings that can remain fully operational during and after an earthquake. On the other hand, we have no such certainty regarding the performance potential of buildings built 30 or 40 years ago. Some buildings from that era have failed, or will fail, in a catastrophic brittle manner during a seismic event, mainly because the concepts of ductility and energy dissipation were not well understood at the time. In contrast, the 2005 National Building Code of Canada lays out stringent seismic design guidelines, encompassing a wide range of performance criteria, with specifications relating to ductility requirements, and detailed steps for derivation of the earthquake demand. If buildings that were built several decades ago were assessed according to today's design codes, many of them would be considered inadequate. In addition, some recently built structures may also have deficiencies as a result of design or construction errors. Many such structures exist throughout the world and are still in use. There is thus an urgent need to assess and upgrade these structures to resist expected seismic events. Although most failures during an earthquake have been observed to occur in the columns of framed structures, structures with beams deficient in shear do exist and require study.



Elevation of Structure: 80 m (262 ft) high



Floor Plan

All dimensions in m (1 m = 3.28 ft)

Fig. 1—Typical structural layout of cement plant tower.

ACI Structural Journal, V. 104, No. 3, May-June 2007.

MS No. S-2006-132.R1 received August 17, 2006, and reviewed under Institute publication policies. Copyright © 2007, American Concrete Institute. All rights reserved, including the making of copies unless permission is obtained from the copyright proprietors. Pertinent discussion including author's closure, if any, will be published in the March-April 2008 ACI Structural Journal if the discussion is received by November 1, 2007.

Kien Vinh Duong is a Structural Designer at Halcrow Yolles, Toronto, Ontario, Canada. He received his MAsC in 2006 from the University of Toronto, Toronto.

Shamim A. Sheikh, FACI, is a Professor of civil engineering at the University of Toronto. He is a member and Past Chair of Joint ACI-ASCE Committee 441, Reinforced Concrete Columns, and a member of ACI Committee 374, Performance-Based Seismic Design of Concrete Buildings. In 1999, he received the ACI Structural Research Award for a paper on the design of ductile concrete columns. His research interests include earthquake resistance and seismic upgrade of concrete structures, confinement of concrete, use of FRP in concrete structures, and expansive cement and its applications.

Frank J. Vecchio, FACI, is a Professor of civil engineering at the University of Toronto. He is a member of ACI Committees 441, Reinforced Concrete Columns, and 447, Finite Element Analysis of Concrete Structures. He received the 1998 ACI Structural Research Award and the 1999 ACI Structural Engineering Award. His research interests include advanced constitutive modeling and analysis of reinforced concrete, assessment and rehabilitation of structures, and response under extreme load conditions.

Consider, for example, the cement plant preheater tower structure depicted in Fig. 1. It was constructed in 1999, nominally in accordance with ACI code specifications. In subsequent design reviews, a number of deficiencies were uncovered including: 1) the shear reinforcement amounts provided in some of the beams were inadequate to develop the beams' full flexural capacities; 2) the beams' longitudinal reinforcement did not fully penetrate the column joints as required by seismic detailing provisions, but rather was terminated short (refer to Fig. 2); and 3) in the lower story columns, the lateral confining reinforcement was inadequate with respect to its amount and spacing. Similar details have been used for a number of such structures recently constructed throughout the Americas. These and other deficiencies rendered the structure's expected performance under design seismic conditions highly questionable—likely inadequate and potentially catastrophic. The structure is currently being

rehabilitated, including the strengthening of beams for shear using CFRP wrap.

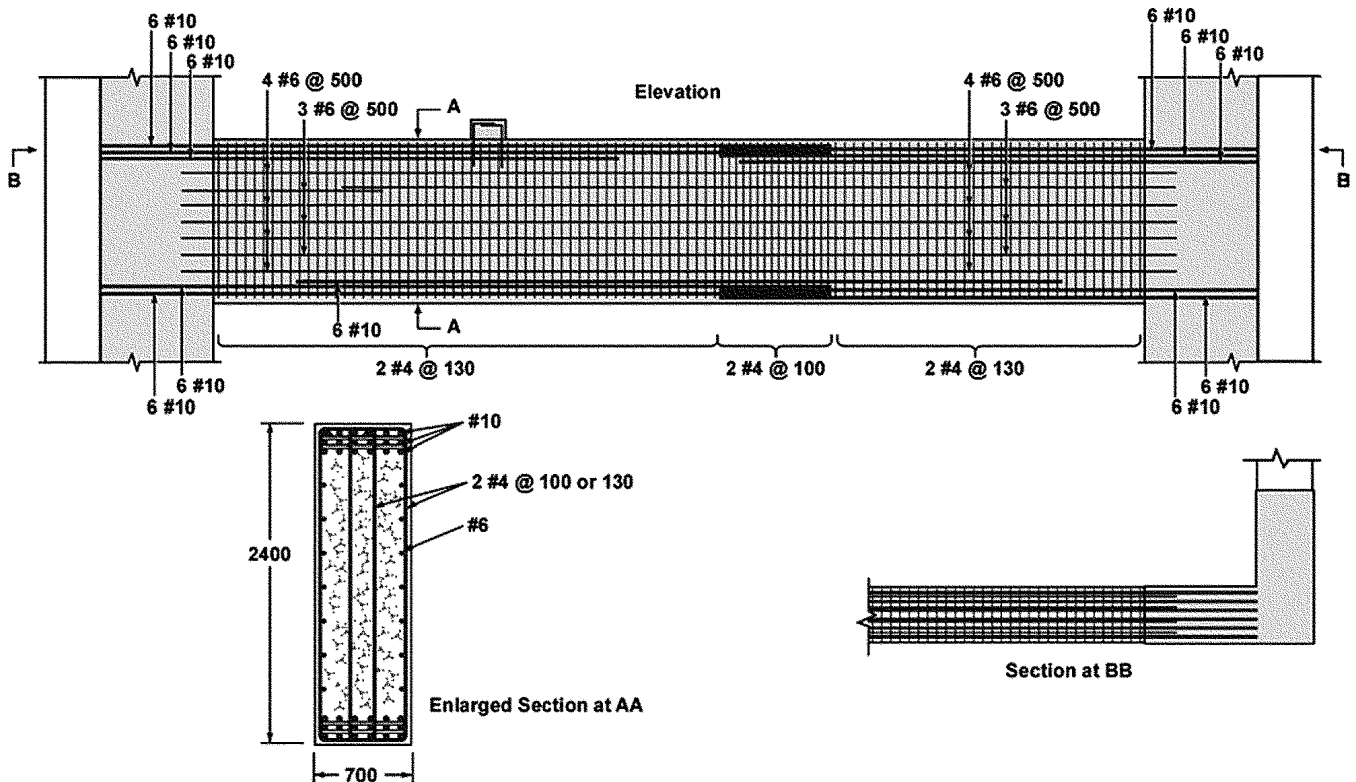
RESEARCH SIGNIFICANCE

Reinforced concrete framed structures that are deficient in shear, particularly in respect to the beams, have not been adequately studied, although some work in the area has been reported.¹⁻³ Unlike in moment-critical buildings where the flexural failure is ductile, shear-critical failures are usually associated with much less forgiving brittle mechanisms, usually with little forewarning. The goal of the research project described herein was to not only increase the knowledge of how shear-critical reinforced concrete structures behave, but also to provide much needed experimental data for further theoretical and analytical development in this area. A better understanding of the behavior of shear deficient structures will allow engineers to properly evaluate and accordingly retrofit these structures before failure takes place. The work reported herein is a summary of the investigation for which the details are available elsewhere.⁴

EXPERIMENTAL PROGRAM

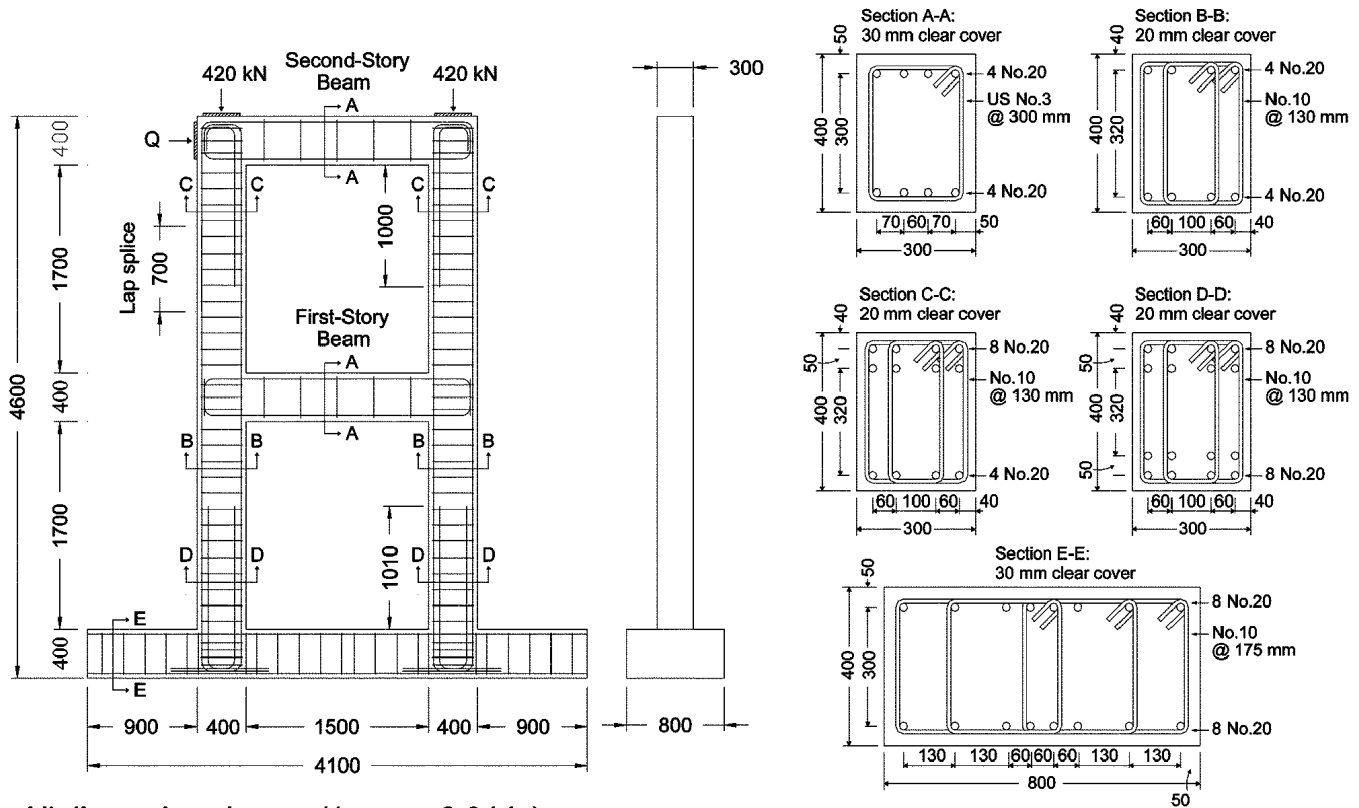
Test specimen

A single-span, two-story, reinforced concrete frame with shear-critical beams was constructed and tested. The frame was designed to replicate, as much as possible, details in the preheater tower structure described previously, in aspects relating to expected shear response. Hence, the test frame attempted to conform to the tower's details in relation to beam span-to-depth ratio, shear reinforcement amounts, longitudinal reinforcement amounts, and material strengths. No attempt was made to replicate the details of the beam's



All dimensions in mm (1 mm = 0.04 in)

Fig. 2—Typical reinforcement details of cement plant tower.



All dimensions in mm (1 mm = 0.04 in.).

Fig. 3—Details of test frame.

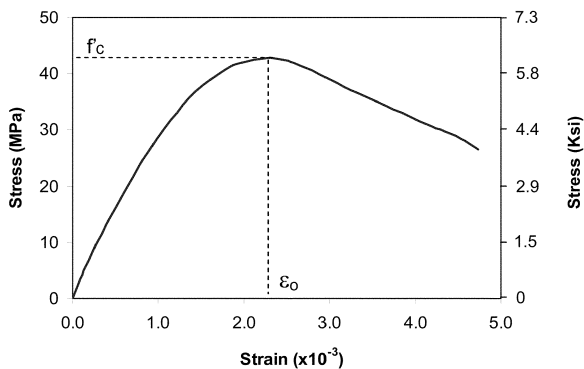


Fig. 4—Concrete stress-strain relationship at 9 months (time of testing).

Table 1—Steel reinforcement material properties

Bar Size	Diameter, mm (in.)	Cross-sectional area, mm ² (in. ²)	ϵ_{y_s} , $\times 10^{-3}$	ϵ_{sh} , $\times 10^{-3}$	f_y , MPa (ksi)	f_u , MPa (ksi)	E_s , MPa (ksi)	E_{sh} , MPa (ksi)
No. 10	11.3 (0.44)	100 (0.16)	2.38	22.8	455 (66)	583 (84.6)	192,400 (27,904)	1195 (173)
No. 20	19.5 (0.77)	300 (0.47)	2.25	17.1	447 (64.8)	603 (87.5)	198,400 (28,774)	1372 (199)
US No. 3	9.5 (0.375)	71 (0.11)	2.41	28.3	506 (73.4)	615 (89.2)	210,000 (30,457)	1025 (149)

longitudinal reinforcement anchorage and the column's confining reinforcement; rather, it was felt that the test model would yield more useful information if these aspects were removed. The only deficiency in the test frame was the inadequate shear reinforcement in the beams.

Table 2—Cross-sectional details of frame components

Member	b , mm (in.)	h , mm (in.)	Bottom steel	Top steel	Stirrup spacing	$\rho_x(A_s/bd)$, %	ρ_y , %
Beam	300 (11.8)	400 (15.7)	4 No. 20	4 No. 20	US No. 3 at 300 mm (single hoop)	1.143	0.158
Column	300 (11.8)	400 (15.7)	4 No. 20	4 No. 20	No. 10 at 130 mm (double hoop)	1.111	1.018
Column (at base)	300 (11.8)	400 (15.7)	8 No. 20	8 No. 20	No. 10 at 130 mm (double hoop)	2.39	1.018
Base	800 (31.5)	400 (15.7)	8 No. 20	8 No. 20	No. 10 at 175 mm (triple hoop)	0.857	0.429

The test frame stood approximately 4.6 m (15.1 ft) tall and 2.3 m (7.55 ft) wide (refer to Fig. 3 for details). The beams were nominally 300 mm (11.8 in.) wide by 400 mm (15.7 in.) deep. The columns also had dimensions of 300 x 400 mm (11.8 x 15.7 in.). To provide fixity at the bottom, a reinforced concrete base 800 mm (31.5 in.) wide, 400 mm (15.7 in.) thick, and 4100 mm (13.5 ft) long was built integrally with the body of the frame and post-tensioned to the strong floor prior to testing. The beam clear span was 1500 mm (4.9 ft) and the column clear story height was 1700 mm (5.6 ft). The concrete used was 43 MPa (6240 psi) with 10 mm (0.4 in.) maximum sized aggregates. Refer to Fig. 4 for the concrete stress-strain response.

The frame was tested in a lateral reverse cyclic manner until severe shear damage took place in the beams. The beams were then repaired with carbon fiber-reinforced polymer (CFRP), and the frame was retested.

Reinforcement

Three types of steel reinforcement were used in the construction of the test frame: No. 10 (100 mm² [0.16 in.²] area), No. 20 (300 mm² [0.47 in.²] area), and US No. 3 (71 mm² [0.11 in.²] area). Typical beam and column sections contained four No. 20 bars as top and bottom reinforcement, with US No. 3 closed stirrups spaced at 300 mm (11.8 in.) in the beams and No. 10 double closed hoops spaced at 130 mm (5.1 in.) in the columns. The base section contained eight No. 20 top and bottom bars, with No. 10 triple closed hoops spaced at 175 mm (6.9 in.). Refer to Fig. 5 for the reinforcement stress-strain responses. Tables 1 and 2 show the steel properties and the reinforcement details of frame components, respectively. Clear covers of 30 mm (1.2 in.), 20 mm (0.8 in.), and 40 mm (1.6 in.) were used for the beams, columns, and base, respectively.

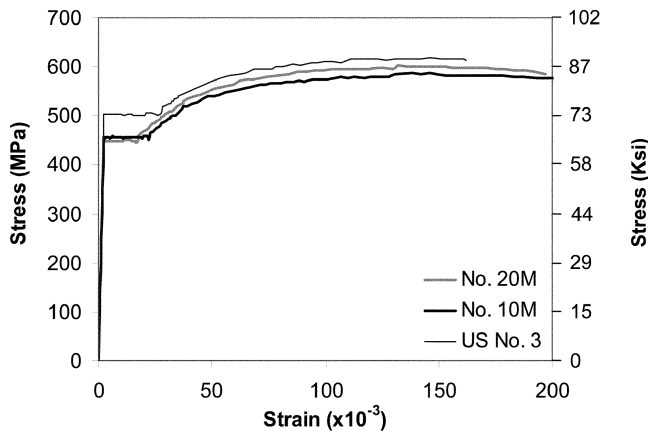


Fig. 5—Reinforcement stress-strain relationship.

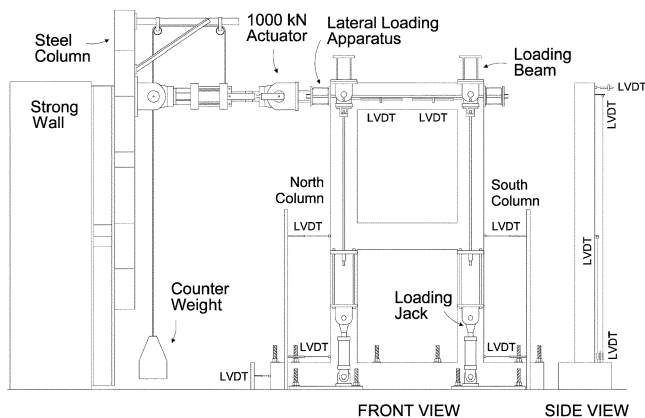
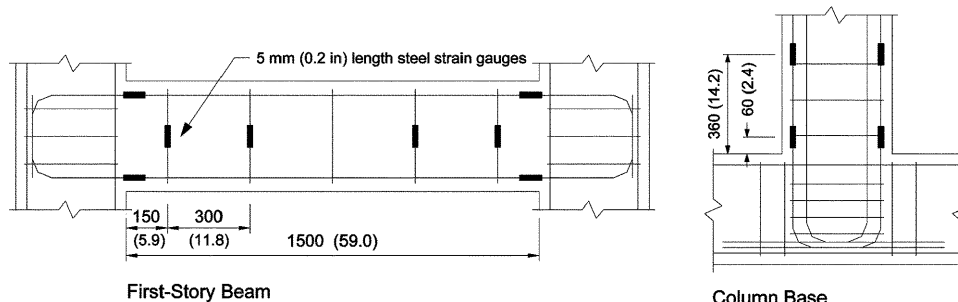


Fig. 6—Test setup.



All dimensions in mm (in.).

Fig. 7—Steel strain gauge layout.

Carbon fiber-reinforced polymer

A commercially-available composite system was used to repair the damaged specimen. The fabric consisted of high strength carbon fibers orientated in the longitudinal direction and sparsely spaced weft in the transverse direction. A thermoset epoxy resin was used for the bonding of the CFRP. The material properties of the composite are summarized in Table 3. The thickness of the CFRP composite was approximately 1 mm (0.04 in.).

Test setup

The testing assembly consisted of vertical and lateral loading systems, as well as an out-of-plane bracing system (refer to Fig. 6). Vertical column loads were applied through four hydraulic jacks (two jacks per column) that were mounted to the laboratory strong floor. The axial load of 420 kN (94.4 kips) per column (210 kN [47.2 kips] per jack) was applied at the top story and held constant throughout the test in a force-controlled manner. The column axial load was $0.065f'_cA_g$, which was similar to the load on the columns of the prototype structure. Horizontal loading was applied using a displacement-controlled actuator positioned at the top story beam centerline. This actuator was anchored against a strong wall and had a load capacity of 1000 kN (224.8 kips) and a stroke capacity of approximately ± 165 mm (6.5 in.) after accounting for slack in the loading system. For consistency, the lateral load was applied in such a manner that the frame was always being pushed regardless of the load direction. A loading apparatus was fabricated to induce a compression force in the top story beam when either a forward or reverse load was applied. The level of axial compression was small enough not to affect the shear behavior of the beams in any significant manner.⁴

Instrumentation

Two types of strain gauges were used in this experiment: 5 mm (0.2 in.) long gauges for reinforcing steel and 60 mm (2.4 in.) long gauges for CFRP. Readings from the two types of strain gauges were used to correlate reinforcing bar or CFRP stresses in the experiment. A total of 36 steel strain gauges were mounted on the longitudinal reinforcement, at potential locations for beam and column flexural hinging, and on the beam stirrups (Fig. 7). Both beams employed the

Table 3—CFRP material properties

Product	f'_t , MPa (ksi)	E_c , MPa (ksi)	ϵ_{ult}^y , $\times 10^{-3}$	Laminate thickness, mm (in.)
CFRP wrap	876 (127)	72,400 (10,500)	12.1	1.0 (0.4)

Note: Material properties were provided by manufacturer and were based on ASTM D 3039⁹ standard coupon tests and laminate thickness of 1.0 mm.

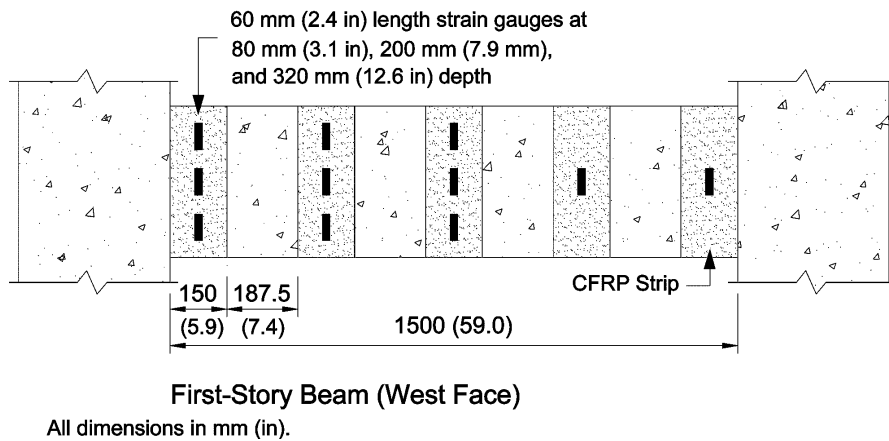


Fig. 8—CFRP layout.

same steel strain gauge layout, as did both column bases. Thirty-two CFRP strain gauges were attached to the surface of 10 evenly-spaced CFRP strips (five strips per beam) (refer to Fig. 8). On the west face of the beams, 10 strain gauges were applied at the middepth, along the vertical centerline of each strip. In addition, top and bottom strain gauges at 320 and 80 mm (12.6 and 3.1 in.) depth, were attached to several CFRP strips as illustrated. The strain gauge layout of the top story beam is a mirror image of Fig. 8. On the east face of the beams, 10 gauges were applied at the middepth of each strip.

Small circular metal studs approximately 10 mm (0.4 in.) in diameter were attached to the concrete surface and used to measure concrete surface strains during testing. Vertical, horizontal, and diagonal surface strains were recorded between targets arranged in a 300 x 300 mm (11.8 x 11.8 in.) grid along the columns and beams. All targets were situated 50 mm (2 in.) from the outer concrete edge, which represented the approximate location of the longitudinal reinforcement in the specimen.

Seventeen linear variable differential transducers (LVDTs) were placed at various locations, as illustrated in Fig. 6. The frame's lateral displacement was recorded at the top story, first story, and base levels. In addition, the top- and first story beam elongations and potential base slip were recorded. Column axial shortening and elongating was monitored at the top story, first story, and bottom of both columns.

Loading sequence

Two phases of loading were carried out: Phase A for a single cycle consisting of forward and reverse loading, and Phase B for a sequence of complete cycles at multiples of the yield displacement. In Phase A, the frame was loaded in the forward direction (forward half-cycle) until significant shear damage occurred, returned back to zero displacement, loaded in the reverse direction (reverse half-cycle) to the same displacement amplitude reached in the forward half-cycle, then unloaded. This phase of testing took 5 days to complete and 26 load stages to record. At early load stages, the horizontal load was held constant while data such as crack widths and Zurich readings were gathered; however, at later load stages, the load was reduced to approximately 80% for safety. The steel strains and LVDT readings were recorded continuously throughout via the computer. At the end of each day, the horizontal load was released, while the vertical load was held constant. At the beginning of the following day, the horizontal load was brought back to the original level from the previous load stage.

During the forward half-cycle of Phase A, load stages were taken at increments of 25 kN (5.6 kips) or at important changes in structural behavior (for example, first cracking and sudden propagation in crack width). During the reverse half-cycle of Phase A, a larger load increment of approximately 30 kN (6.7 kips) was adopted. The widths of only prominent crack widths were measured, and Zurich readings were only recorded at selected load stages.

Repair of the beams was carried out between Phase A and B. The repair procedure involved chipping off unsound concrete in the two beams, grouting large voids using a shrinkage-compensated microsilica-enhanced wet mortar with compressive strength similar to the specimen, and pressure injecting epoxy into the cracks. The repaired concrete surface was ground and smoothed out in preparation for CFRP wrapping. The CFRP configuration consisted of five fully-wrapped strips that were 150 mm (5.9 in.) wide and equally spaced along the length of each beam (Fig. 8). An overlap at the top surface of approximately 75 mm (3 in.) was used in all the CFRP strips. The criterion used for the design of CFRP stirrups was that flexural hinging of beams should develop prior to any shear failure. It should be noted that conditions in the field structure were such that a complete wrap of CFRP sheets around the beams was possible. Also, although commercially available proprietary CFRP materials were used in this research, any structural FRP system could be used to provide the required strengthening of the beams.

In Phase B, 12 load cycles were applied at various increments of the yield displacement. Seven days were devoted to this phase of testing. Load cycles were performed in the following sequence: two load cycles each of $\pm 0.75\Delta_y$, $\pm 1.0\Delta_y$, $\pm 2.0\Delta_y$, $\pm 3.0\Delta_y$ displacement amplitude, and four cycles of $\pm 4.0\Delta_y$.

The yield displacement Δ_y was determined from Phase A to be 25 mm (1.0 in.). This displacement corresponded to the approximate first yielding of the flexural reinforcement in the first story beam of the test specimen, as measured by strain gauges. The yield displacement represented an overall frame drift of 0.625%. Following the fourth cycle at $\pm 4.0\Delta_y$, the frame was pulled until the actuator stroke limit was reached. This corresponded to a frame displacement of $-6.6\Delta_y$ or -164 mm (-6.5 in.). In the initial and intermediate load stages, creep effects resulted in slight drops in load. At later load stages, drops in force were primarily due to the propagation of large shear cracks. Creep effects were similar in both

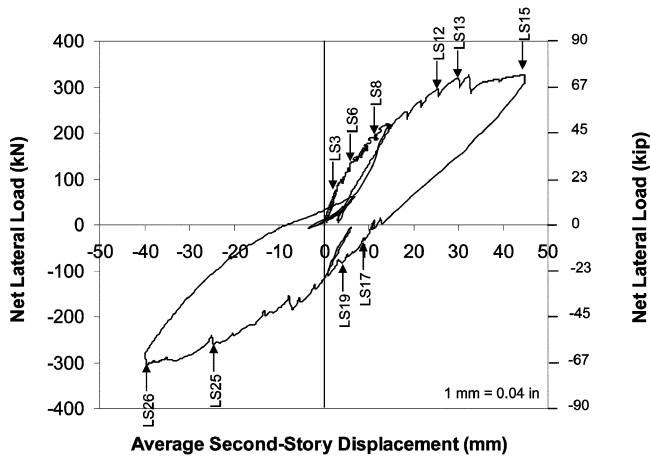


Fig. 9—Lateral load versus top story displacement (Phase A).

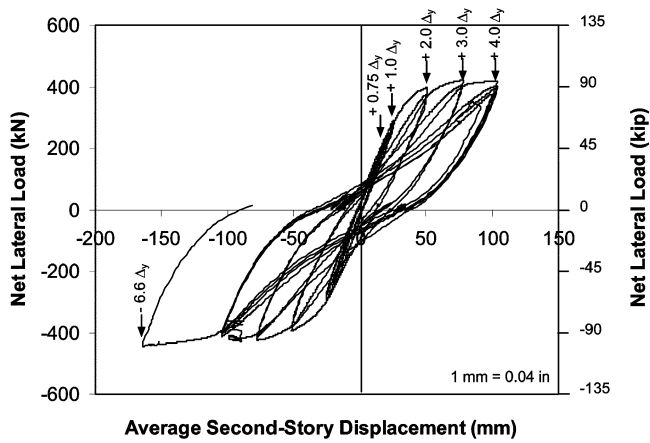


Fig. 10—Lateral load versus top story displacement (Phase B).

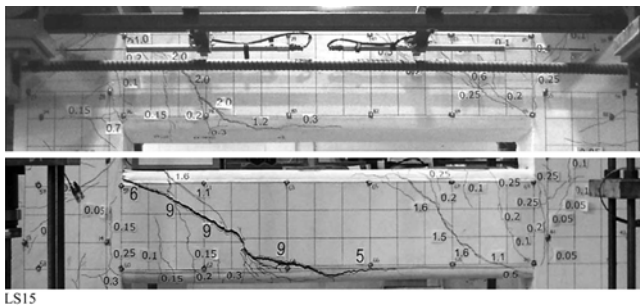


Fig. 11—Frame at peak forward half-cycle (Phase A).

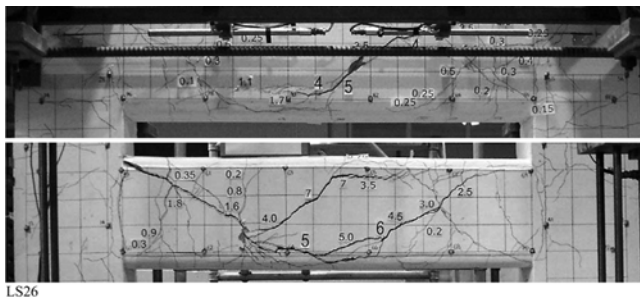


Fig. 12—Frame at peak reverse half-cycle (Phase A).

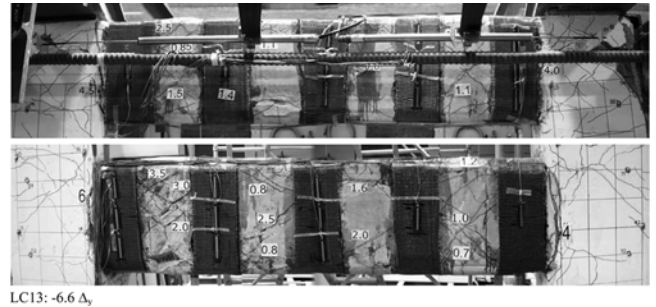


Fig. 13—Frame at peak reverse cyclic load displacement (Phase B).



Fig. 14—Overall frame deformation at peak reverse half-cycle (Phase A).

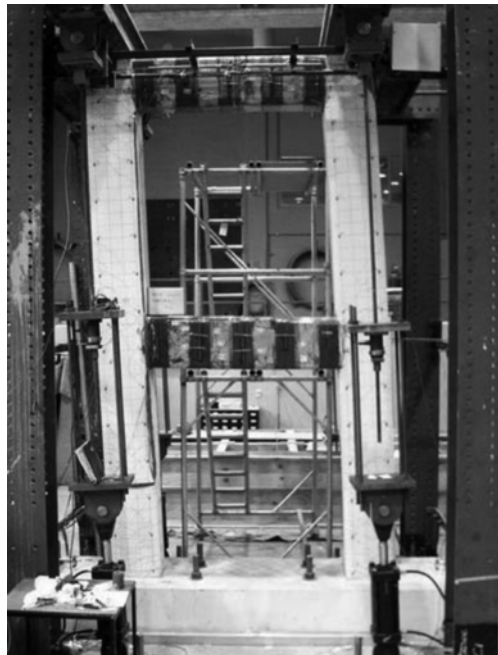


Fig. 15—Overall frame deformation at peak reverse cyclic load displacement (Phase B).

phases of the tests and had no significant influence on the overall behavior of the frame.

TEST RESULTS

Test observations—Phase A

The overall load deformation responses of the test frame during Phase A and B of testing are summarized in Fig. 9 and 10, respectively. The lateral loads in the figures have been corrected for P-delta effects. Key load stages and load cycles are indicated. Key cracking patterns are shown in Fig. 11 through 13. The overall frame deformations after each phase of testing are presented in Fig. 14 and 15.

In the forward half-cycle of Phase A, the maximum lateral load applied was approximately 327 kN (73.5 kips) (LS15) with a corresponding average top story lateral displacement of 44.7 mm (1.8 in.). The damage mode was combined flexural-shear. Lower and upper beam flexural cracks were first observed at 75 kN (16.9 kips) (LS3), followed by a lower beam shear crack at 148 kN (33.3 kips) (LS6). At 197 kN (44.3 kips), flexural cracks at both ends of the upper and lower beams stabilized while the lower beam shear crack widened. In addition, several new shear cracks developed at the top story beam during this load stage. At approximately 295 kN (66.3 kips) (LS13), the first-story beam longitudinal steel yielded in flexure at both ends. Stirrups at the first-story beam yielded shortly after at 320 kN (71.9 kips) (LS13). At the most heavily damaged state, the largest shear crack at the first-story beam reached 9 mm (0.35 in.) wide, while the largest shear crack at the top story beam reached 2 mm (0.1 in.) wide. Flexural cracks were at most 0.25 mm (0.01 in.) wide. The tensile steel stresses at the column bases were less than half of yield throughout the forward half-cycle.

Upon unloading from the forward half-cycle at zero horizontal force, the frame exhibited approximately 11 mm (0.43 in.) of top story residual lateral deflection. The test specimen was pulled in the reverse direction to approximately the peak displacement reached during the forward half-cycle (approximately 40 mm [1.6 in.]). Unlike the forward half-cycle where the damage mode was combined flexural-shear, the frame under reverse loading sustained mostly shear damage. At the conclusion of the reverse half-cycle, a peak horizontal load of -304 kN (-68.3 kips) (LS26) was reached with an average top story lateral displacement of -39.5 mm (-1.6 in.). Lower and upper beam flexural cracks were developed at -32 kN (-7.2 kips) (LS17), while the lower beam shear cracks appeared at -84 kN (-18.9 kips) (LS18). In general, the crack development was discontinuous and abrupt. Because of the numerous cracks generated from the forward half-cycle, the cracks developed during the reverse half-cycle were largely interrupted and uneven. The sudden propagation of cracks was also a common behavior. At -260 kN (-46.3 kips) (LS25), the stirrups in the lower beam yielded. At the peak load of -304 kN (-68.3 kips) (LS26), the largest shear cracks at the lower and upper beams were 7 and 5 mm (0.28 and 0.2 in.) wide, respectively. The beam flexural steel was near yield at 430 MPa (62.4 ksi) (approximately 95% of yield). The column flexural steel stress was less than half of yield stress. Beam and column flexural cracks were minor in comparison with the beam shear cracks. At the end of this loading phase, the lateral load was reduced and the frame was pushed forward to a displacement where the residual lateral deflection upon unloading was approximately zero. Figure 9 provides information on residual conditions after unloading at the end of Phase A.

Test observations—Phase B

After CFRP repair of the two beams, the frame was loaded in a reversed cyclic manner. The test frame developed a full plastic hinge failure mechanism. Strain and deformation readings and visual observations showed that hinges were formed at the four beam ends and at the two column bases. The peak lateral load reached was -444 kN (-99.8 kips), which corresponded to an average top story displacement of -164 mm (-6.5 in.) (-6.6 Δ_y). This displacement represented the limit of actuator stroke rather than that of the frame. There was no indication of impending collapse of the frame.

Shear cracks in both beams were first observed at $\pm 0.7\Delta_y$. Flexural interface cracks at all four ends of the two beams were developed shortly after at $\pm 1.0\Delta_y$. At $\pm 3.0\Delta_y$, the shear cracks were approximately 1.5 mm (0.06 in.) wide, while the flexural interface cracks were 3.5 mm (0.14 in.) wide. Flexural hinges at the beam's ends were fully developed at this displacement. In addition, shear cracks were also apparent at the top story beam-column joints. At $\pm 4.0\Delta_y$, the beam shear cracks were 2.5 mm (0.1 in.) wide, the column base flexural cracks were 1.5 mm (0.06 in.) wide, and the column base concrete cover was spalling. Due to excessive damage of the two concrete beams, the test frame was slightly twisting out-of-plane. At the final load cycle at -6.6 Δ_y , the beam shear cracks were 3.5 mm (0.14 in.) wide, while the beam interface flexural cracks reached a maximum of 6 mm (0.24 in.). The concrete cover at the top story beam-column joints was partially spalled off.

Steel strain

From the monitoring of strains in the steel, the following observations were made. For the beam shear reinforcement, during Phase A, the stirrups at the lower story beam yielded towards the end of the forward and reverse half-cycles at LS13 and LS25, respectively. During Phase B, even though a full flexural plastic hinge mechanism had developed, the stirrups at the first and top story beams also yielded. The stirrups at both ends of the lower beam and at the north end of the upper beam yielded at $\pm 2.0\Delta_y$, while the stirrup at the south end of the upper beam yielded at $\pm 3.0\Delta_y$.

For the beam flexural reinforcement, during the forward half-cycle of Phase A, the lower and upper beam flexural steel yielded at LS12 (295 kN [66.3 kips]) and LS13 (320 kN [71.9 kips]), respectively. In Phase B, the longitudinal flexural steel in the lower beam yielded in tension at approximately $\pm 1.0\Delta_y$, while the longitudinal flexural steel in the upper beam yielded in tension at approximately $\pm 2.0\Delta_y$. The longitudinal steel in the beams did not yield in compression. The column steel yielded in both tension and compression at the base when displacements of $\pm 3.0\Delta_y$ were reached. At the end of LC13, the longitudinal flexural steel at the column bases did not reach strain hardening.

Strain in CFRP

When strains in the CFRP were examined, it was observed that the majority of CFRP strains at the lower beam exceeded the design strain limit of 4000×10^{-6} recommended by ISIS Canada.⁶ The majority of the strains in the upper beam remained below 4000×10^{-6} up to LC13 (-6.6 Δ_y), when one reading exceeded this limit. For a fully wrapped beam, such as in this specimen, the term debonding meant that the CFRP-concrete interface adhesion was breaking, but the wrap was still intact and provided near-full shear resistance. Partial CFRP debonding was initiated at the lower beam at

LC5 ($\pm 2.0\Delta_y$). At the $\pm 4.0\Delta_y$ cycles, all of the CFRP wraps at the lower beam exhibited debonding of more than 50% of their original bonded area. Partial debonding took place at the upper beam at $\pm 4.0\Delta_y$. The CFRP strains increased slightly when the top displacement increased from $-4.0\Delta_y$ to $-6.6\Delta_y$, but not at the same rate as the increase from $\pm 3.0\Delta_y$ to $\pm 4.0\Delta_y$. The maximum CFRP strain recorded was approximately 6200×10^{-6} located at the second strip from the north end of the lower beam. In the upper beam, with the exception of a strip located at the south end where the strain was 4300×10^{-6} , the maximum CFRP strain recorded was approximately 3800×10^{-6} . No sign of CFRP rupture was observed at any location in the beams.

DISCUSSION OF RESULTS

Overall frame behavior

Table 4 compares the results of the test frame during Phase A and Phase B of the experiment. The performance of the repaired frame was much more suitable for earthquake design than that of the original frame. Substantial improvements were exhibited in all aspects of the response. The peak lateral load increased by a factor of approximately 1.4 to 444 kN (99.8 kips); the displacement ductility, as calculated using the method suggested by Sheikh and Houry,⁷ improved from approximately 4.0 to at least 6.8, an increase by a factor of at least 1.7; the maximum displacement increased by a factor of at least 3.7; while the energy dissipation increased by a factor of at least 5.7. Recall that, for Phase A, although failure of the frame did not take place, the load capacity had leveled off and the frame exhibited large beam shear cracks that suggested failure was imminent. Therefore, the ductility and maximum displacement reported were very close to the final values. Contrarily, for Phase B, the peak load and displacement were reached at the end of the last load cycle ($-6.6\Delta_y$) where the test was stopped not by the limitation of the test specimen, but by the limitation of the actuator stroke capacity. Therefore, the maximum displacement and ductility were not fully realized; the values reported are thus lower limits.

CFRP strain limits suggested by ISIS Canada

Experimental observations suggested that partial debonding took place at several wraps at the lower beam during Load Cycle LC5 ($+2.0\Delta_y$), and at the upper beam during Load Cycles LC9 through LC12 ($+4.0\Delta_y$). The CFRP strain gauges indicated that when partial debonding occurred, the maximum CFRP strains reached were approximately 3000×10^{-6} . It was difficult to quantify the degree of debonding because the beam was fully wrapped; however, physical examination of the CFRP wraps concluded that, for the wraps that exhibited partial debonding at the load stages mentioned previously, approximately 10 to 15% of their bonded area was broken. During LC9 ($+4.0\Delta_y$), inspection of the lower beam revealed that more than 50% of the bonded area for each wrap was broken. The CFRP strains recorded in the lower beam were, on average, approximately 4000×10^{-6} . If the wraps were not properly anchored, they would have likely ripped off at this stage. At LC13 ($-6.6\Delta_y$), further debonding took place at the upper beam; the majority of strains recorded here ranged between 3000×10^{-6} and 4000×10^{-6} . Recall that the CFRP strains were recorded at the vertical centerline of the wraps (that is, where the gauges were installed). The variation of strain along the width of each wrap was unknown. Taking this limitation into consideration, it was concluded that the CFRP-concrete interface exhibited partial

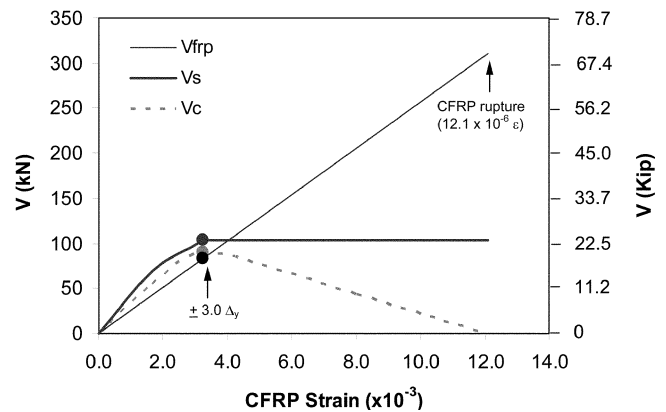


Fig. 16—Shear strength (V_c , V_s , and V_{frp}) versus CFRP strain.

Table 4—Cyclic response of test specimen

	Phase A	Phase B
V_{peak} , kN (kips)	327 (73.5)	444 (99.8)
δ_y , mm (in.)	11 (0.43)	24 (0.94)
δ_{max} , mm (in.)	44 (1.73)	164 (6.5)
$^*\mu_{\Delta} = \delta_{max}/\delta_y$	~4.0	>6.8
V_{peak} increase	~1.4 × original	
δ_{max} increase	>3.7 × original	
μ_{Δ} increase	>1.7 × original	
Energy dissipation	>5.7 × original	
V_f , kN (kips)	202 (45.4)	>264 (59.4)
V_s , kN (kips)	103 (23.1)	103 (23.1)
V_c , kN (kips)	99 (22.3)	>78 (17.5)
V_{frp} , kN (kips)	—	83 (18.7)

debonding when the CFRP strain at the wrap vertical centerline reached approximately 3000×10^{-6} , while more than 50% of the area had debonded when a strain of approximately 4000×10^{-6} was reached.

ISIS Canada recommends a strain limit of 4000×10^{-6} when calculating the shear contribution of CFRP for fully wrapped beams.⁶ It suggests that, above this strain limit, the aggregate interlock of the concrete is lost due to widening of the crack. In this experiment, the majority of the strains recorded in the lower beam were in excess of 4000×10^{-6} , but all of the wraps remained intact. This experimental finding indicated that the strain limit placed by ISIS is conservative. In addition, for the type and layout of the CFRP used, the ISIS design manual suggests a rupture strain limit of 5500×10^{-6} .⁶ The maximum CFRP strain recorded in this experiment was 6430×10^{-6} , while several other gauges recorded strains close to 6000×10^{-6} . All of the CFRP wraps were fully intact at the end of the experiment. Again, this recommendation was found to be conservative.

Although a commercially available FRP system was used, it is believed that the results obtained from this study are generally applicable to other FRP systems as long as due consideration is given to the material properties such as strength, stiffness, and rupture strain.

Estimation of V_f , V_c , and V_r in first-story beam

In Phase A, the peak shear force in the first-story beam was estimated using the CSA A23.3 2004 code.⁸ Refer to

Fig. 16 and Table 4. Assuming an induced beam compression force of 40 kN (9.0 kips) from the restraint provided by the columns, as determined from nonlinear finite element analysis, and assuming stirrup yielding as evident from experimental observations, the shear capacity was calculated to be 202 kN (45.4 kips) with $V_c = 98.8$ kN (22.2 kips) and $V_s = 103$ kN (23.2 kips). The calculated strength according to code formulations was taken to be a reliable estimate because the calculation results correlated well to several experimental observations such as the shear failure angle and longitudinal tensile stress. The shear capacity was not sensitive to the axial compression load, as determined from the sectional and finite element analyses.

After repair in Phase B, the total shear resistance V_r of a beam cross section can be calculated as equal to the summation of the concrete shear strength V_c , transverse steel strength V_s , and CFRP strength V_{frp}

$$V_r = V_c + V_s + V_{frp}$$

The peak shear force V_f acting in the first-story beam, corresponding to conditions at $+3.0\Delta_y$, was estimated using hand calculations and experimental observations. To calculate the shear force V_f the tip of the plastic hinge region at 150 mm (5.9 in.) away from the beam-column support was assumed to reach the yield moment M_y . The stirrups had yielded, but did not reach strain hardening because the CFRP wrap provided vertical confinement that limited the increase in the stirrup strain. With an estimated induced compressive force of 40 kN (9.0 kips) (from Phase A), M_y and V_f were calculated to be 159 and 265 kN-m (117.3 and 194.7 kip-ft.), respectively. Using the average stress of the CFRP wraps ($\sigma_{frp} = 200$ MPa [29 ksi]) along the lower beam, and taking an average of the stresses between the forward and reverse cycles, V_{frp} was estimated to be 83.4 kN (18.7 kips). Setting V_f equal to V_r , the peak V_c calculated was 77.6 kN (17.4 kips) in Phase B, which was approximately 20% lower than the V_c of 98.8 kN (22.2 kips) obtained in Phase A at failure.

It is important to illustrate the sensitivity of the plastic hinge region on the V_f calculation. The moment at 150 mm (5.9 in.) away from the beam-column interface was assumed conservatively to reach M_y . If the plastic hinge region extended by a length equal to the beam depth of 400 mm (15.7 in.) and M_y was assumed herein, V_f would equal 453 kN (101.8 kips) and V_c would equal 267 kN (60.0 kips). The concrete shear strength would increase as a result of the confining pressures of the CFRP, but even so, a concrete shear strength of 267 kN (60.0 kips) appears to be unrealistic. If the clear span of the beam is used to calculate beam shear, the contribution of the concrete is only 26 kN (5.8 kips). The lower limit of the actual concrete shear strength V_c is confidently estimated at 77.6 kN (17.4 kips).

The ultimate shear resistance of the repaired beam was also estimated by assuming yielding of the stirrup and rupture of the CFRP (12.1×10^{-3}) while conservatively neglecting the V_c contribution. At a strain level of 12.1×10^{-3} , large shear cracks in the beam significantly reduce the concrete shear strength. Even though the CFRP-concrete interface will break prior to rupture, the CFRP can still carry the load because of its fully-wrapped configuration.⁹ The total shear resistance was estimated to be 414 kN (93 kips). Figure 16 illustrates various shear strengths versus CFRP strain. The dotted lines represent rough estimates of the behavior. The

three points shown were the V_{frp} , V_s , and V_c values calculated at $+3.0\Delta_y$.

CONCLUDING REMARKS

A large-scale two-story one-bay test frame, with shear deficient beams, was constructed and tested under reversed cyclic lateral loads while the columns were subjected to constant axial loads. After the beams were severely damaged during the first load cycle, they were repaired with CFRP wrap and tested again under increasing lateral displacement.

The test results indicate that the beams in the test frame were subject to brittle shear failure at displacement amplitudes of little over $1.0\Delta_y$. Upon repair, the damage mode changed from brittle flexural-shear to ductile flexure. The displacement ductility improved by a factor of more than 1.7, the maximum displacement increased by a factor of more than 3.7, and the energy dissipation increased by a factor of more than 5.7. After repair, the beam's shear capacity increased by at least 30%, with the CFRP contributing to 30% of the total shear strength. The repaired concrete shear contribution V_c was at least 80% of the original strength. These numbers represent the lower limits for the enhancements due to FRP repair because the test was terminated due to actuator limitation and not as a result of failure of the frame.

The *ISIS Design Manual*⁶ is conservative in its estimation of both the upper CFRP strain limit and the CFRP rupture strain. For future experimental work, it is recommended that the flexural capacity of the beams be increased to achieve shear rupture in the CFRP wrap.

The test program also clearly showed that, for frame structures that have been constructed with inadequate shear reinforcement in the beams, the prospects of brittle catastrophic failure during seismic events are significant. Such failures can occur at displacement ductility ratios of 1.0 or less. Tools and techniques for assessment and rehabilitation of these structures are much needed.

ACKNOWLEDGMENTS

The research reported herein was supported by grants from the Natural Sciences and Engineering Research Council of Canada (NSERC) and ISIS Canada, an NSERC Network of Centers of Excellence. The additional material and technical support provided by the Vector Construction Group and Fyfe Co. is gratefully acknowledged. Experimental work was carried out in the Structures Laboratories of the University of Toronto.

NOTATION

A_s	= cross-sectional area of tensile longitudinal steel reinforcement
A_v	= cross-sectional area of transverse steel reinforcement (stirrups)
b	= web width
d	= distance from extreme compression fiber to centroid of longitudinal tension reinforcement
E	= elastic modulus of concrete
E_s	= elastic modulus of steel
E_{sh}	= elastic modulus of steel at strain hardening
f'_c	= specified compressive strength of concrete
f'_t	= specified tensile strength
f_u	= ultimate stress of steel reinforcement
f_y	= yield stress of steel reinforcement
LC	= load cycle (Phase B)
LS	= load stage (Phase A)
M_y	= yield moment
s	= spacing of stirrups
V_c	= shear strength of concrete
V_f	= shear force
V_{frp}	= shear strength of CFRP
V_r	= applied shear resistance
V_s	= shear resistance of reinforcement
Δ_y	= yield displacement determined from cross section
δ_{max}	= maximum displacement (Appendix B)

δ_y = yield displacement determined from tangent stiffness (Appendix B)
 ϵ_o = concrete strain at peak stress
 ϵ_s = tensile strain in longitudinal steel reinforcement
 ϵ_{sh} = tensile strain in longitudinal steel reinforcement at strain hardening
 ϵ_{ult} = ultimate CFRP strain at rupture
 μ = displacement ductility (δ_{max}/δ_y)
 ρ_x = longitudinal tensile steel reinforcement ratio; $\rho_x = A_s/bd$
 ρ_y = transverse steel reinforcement ratio; $\rho_y = A_v/bs$
 σ_{fpp} = stress of CFRP in principle direction

REFERENCES

1. Ozden, S.; Akguzel, U.; and Ozturan, T., "Seismic Retrofit of R/C Frames with CFRP Overlays," *Earth and Environmental Science*, NATO Science Series 29, 2003, pp. 357-382.
2. Vecchio, F. J., and Balopoulou, S., "On the Nonlinear Behavior of Reinforced Concrete Frames," *Canadian Journal of Civil Engineering*, V. 17, No. 5, 1990, pp. 698-704.
3. Vecchio, F. J., and Emara, M. B., "Shear Deformations in Reinforced Concrete Frames," *ACI Structural Journal*, V. 89, No. 1, Jan.-Feb. 1993, pp. 46-56.
4. Duong, K. V., "Seismic Behavior of a Shear-Critical Reinforced Concrete Frame: An Experimental and Numerical Investigation, Research Report," Department of Civil Engineering, University of Toronto, Toronto, Ontario, Canada, 2006, 296 pp.
5. ASTM D 3039/D 3039M, "Standard Test Method for Tensile Properties of Polymer Matrix Composite Materials," ASTM International, West Conshohocken, Pa., 2006, 13 pp.
6. ISIS Canada, "Strengthening Reinforced Concrete Structures with Externally-Bonded Fiber Reinforced Polymers," *Design Manual* No. 4, 2001, 209 pp.
7. Sheikh, S. A., and Houry, S. S., "Confinement of Concrete Columns with Stubs," *ACI Structural Journal*, V. 90, No. 4, July-Aug. 1993, pp. 414-431.
8. Cement Association of Canada, *Concrete Design Handbook*, A23.3-04 Draft, Ottawa, Ontario, Canada, 2004, 358 pp.
9. Sheikh, S. A.; DeRose, D.; and Murdukhi, J., "Retrofitting of Concrete Structures for Shear and Flexure with Fiber Reinforced Polymers," *ACI Structural Journal*, V. 99, No. 4, July-Aug. 2002, pp. 451-459.